Localizing Transformations of the Galaxy-Galaxy Lensing Observable

Youngsoo Park, Eduardo Rozo, and Elisabeth Krause

Phys. Rev. Lett. **126**, 021301 — Published 13 January 2021

DOI: 10.1103/PhysRevLett.126.021301

Localizing Transformations of the Galaxy–Galaxy Lensing Observable

Youngsoo Park
Kavli Institute for the Physics and Mathematics of the Universe (WPI), UTIAS, The University of Tokyo, Kashiwa, Chiba 277-8583, Japan.

Eduardo Rozo
Department of Physics, University of Arizona, AZ 85721, U.S.A.

Elisabeth Krause
Department of Astronomy and Steward Observatory, University of Arizona, AZ 85721, U.S.A.
Department of Physics, University of Arizona, AZ 85721, U.S.A.

(Dated: December 8, 2020)

Modern cosmological analyses of galaxy–galaxy lensing face a theoretical systematic effect arising from the non-locality of the observed galaxy–galaxy lensing signal. Because the predicted tangential shear signal at a given separation depends on the physical modeling on all scales internal to that separation, systematic uncertainties in the modeling of non-linear small scales are propagated outwards to larger scales. Even in the absence of other limiting factors, this systematic effect alone can necessitate conservative small-scale cuts, resulting in significant losses of information in the tangential shear data vector. We construct a simple linear transformation of the standard galaxy–galaxy observable that removes this non-locality, which ensures that the cosmological signal contained within the transformed observable is exclusively drawn from well-understood physical scales. This new observable, through its robustness against non-locality, also enables a significant extension in the range of usable scales in galaxy–galaxy lensing compared to the standard approach in current cosmological analyses.

I. INTRODUCTION

Modern wide-field galaxy imaging surveys [e.g. 1–5] have achieved remarkable success in constraining cosmological parameters from measurements of the late-time matter distribution of our Universe. A promising avenue of recent interest reduces the measured positions and shapes of galaxies to two-point statistics in configuration space and compares those statistics against theoretical predictions for inference. There are three different types of two-point statistics that can be included in such analyses, namely position–position, position–shape, and shape–shape, respectively referred to as galaxy clustering, galaxy–galaxy lensing, and cosmic shear. When making use of these statistics, analysts must determine the range of scales that are modeled accurately enough for cosmological inferences, often in the form of scale cuts. On the small-scale side, the assumed model for the galaxy bias, which relates the spatial distribution of galaxies to that of matter [see e.g. 6, for a review], limits the minimum possible scale that can be used in the analysis. For instance, a perturbative bias model will fail below some minimum physical scale, so comparisons between predictions and observations can only be made outside of that scale, even in the absence of other observational or theoretical systematic effects.

For the case of galaxy–galaxy lensing, the minimum usable scale for analysis can be much larger than the limit discussed above. This is due to the *non-local* nature of the galaxy–galaxy lensing signal, where the predicted signal at a given separation depends on the modeling of *all* scales within that separation, including the non-linear small scales. In galaxy–galaxy lensing, the matter associated with a foreground lens galaxy tangentially distorts the images of background source galaxies. The raw observable is the azimuthally averaged ellipticity of background galaxies tangential to the lens-source separation vector, known as the tangential shear or $\gamma_{\rm t}$. For a lens at redshift $z_{\rm l}$ and a source at redshift $z_{\rm s}$, the tangential shear signal at an observed angular separation θ, or equivalently at a projected comoving spatial separation $R = \theta\chi_{\rm l}$ with $\chi_{\rm l} = \chi(z_{\rm l})$ being the comoving distance to $z_{\rm l}$, is predicted to be

$$\gamma_{\rm t}(\theta|z_{\rm l}, z_{\rm s}) = \frac{\Delta\Sigma(R = \theta\chi_{\rm l})}{\Sigma_{\rm crit}(z_{\rm l}, z_{\rm s})}, \tag{1}$$

where $\Sigma_{\rm crit}(z_{\rm l}, z_{\rm s})$ is a geometric factor given by

$$\Sigma_{\rm crit}(z_{\rm l}, z_{\rm s}) = \frac{c^2}{4\pi G}\frac{(1+z)\chi_{\rm s}}{\chi_{\rm l}(\chi_{\rm s} - \chi_{\rm l})} \tag{2}$$

with $\chi_{\rm s} = \chi(z_{\rm s})$, and $\Delta\Sigma$ being the excess surface density defined as

$$\Delta\Sigma(R) = \overline{\Sigma}(< R) - \Sigma(R). \tag{3}$$

Here, Σ is the projected surface density, i.e.

$$\Sigma(R) = \rho_{\rm m}\int_{-\infty}^{\infty} dR_{\rm z}\xi_{\rm gm}\left(\sqrt{R^2 + R_{\rm z}^2}\right), \tag{4}$$

of matter around the lens galaxy, with $\xi_{\rm gm}$ being the 3D galaxy-matter correlation function and $\rho_{\rm m}$ the comoving mean matter density of the Universe. Note that we exclude the constant background density of matter in our

notation, as it does not induce lensing due to symmetry. $\overline{\Sigma}(< R)$ is the mean surface density internal to R, i.e.

$$\overline{\Sigma}(< R) = \frac{1}{\pi R^2}\int_0^R dR'\ 2\pi R'\ \Sigma(R'). \tag{5}$$

Note that while Σ and $\Delta\Sigma$ implicitly depend on z_l, we choose to suppress this in our notation for simplicity. Equations 3-5 demonstrate that the lensing signal at a radius R, i.e. $\Delta\Sigma(R)$, depends on the surface mass density at all radii interior to R, i.e. $\Sigma(R')$ for $0 \leq R' \leq R$. Consequently, our inability to adequately model the small-scale density field necessarily impacts the lensing signal at *all* scales. This *non-locality* can then force the small-scale cuts applied in real data to be significantly larger than the scale at which theoretical uncertainties in the density field become problematic. This was, for instance, what [7] found from their studies of theoretical systematics for the DES Y1 cosmology analysis.

II. A LOCAL GALAXY–GALAXY LENSING OBSERVABLE

In order to mitigate the non-locality in galaxy–galaxy lensing, one must remove the contribution to the galaxy–galaxy lensing observable from $\xi_{\rm gm}(r)$ on small scales. Several such methods have been discussed, e.g. via subtracting out the estimated contribution from the mass enclosed within some cutoff scale [8, 9] or analytically marginalizing over the said contribution [10]. In this work, we propose a novel approach that is motivated by the local quantity underlying the non-local signal, i.e. the projected surface density $\Sigma(R)$.

The basic idea for our work is that since the surface density contrast $\Delta\Sigma$ is a linear transformation of the local surface density field Σ, inverting this relation would enable us to define an estimator of the surface density field, which would in turn be local. To do so, we begin with the relation between the two:

$$\Delta\Sigma(R) = \frac{1}{\pi R^2}\int_0^R dR'\ 2\pi R'\ \Sigma(R') - \Sigma(R). \tag{6}$$

Differentiating each side with respect to R yields

$$2\pi R\Delta\Sigma(R) + \pi R^2\Delta\Sigma'(R) = -\pi R^2\Sigma'(R), \tag{7}$$

and integrating again from R to $R_{\rm max}$ yields

$$\Sigma(R) = \Sigma(R_{\rm max}) + \int_R^{R_{\rm max}} dR'\ \left[\frac{2\Delta\Sigma(R')}{R'} + \Delta\Sigma'(R')\right]. \tag{8}$$

This is a well-known result [11, 12] which demonstrates that one can reconstruct $\Sigma(R)$ from $\Delta\Sigma(R)$ up to an unknown constant $\Sigma(R_{\rm max})$, typically referred to as the mass sheet degeneracy.

However, we need not concern ourselves with reconstructing the exact $\Sigma(R)$ profile. Our goal here is simply to construct a local galaxy–galaxy lensing observable. To that end, we define a new quantity Y via

$$\begin{aligned} Y(R) &\equiv \Sigma(R) - \Sigma(R_{\rm max}) \\ &= \int_R^{R_{\rm max}} d\ln R'\ \left[2\Delta\Sigma(R') + \frac{d\Delta\Sigma(R')}{d\ln R'}\right]. \end{aligned} \tag{9}$$

From the first line, it is clear that $Y(R)$ is free of contributions from $\xi_{\rm gm}$ on small ($r < R$) scales. From the second line we can see that $Y(R)$ can readily be calculated from $\Delta\Sigma(R')$ for $R \leq R' \leq R_{\rm max}$. Thus, $Y(R)$ is our desired observable.

In a real-life cosmology analysis, observables and predictions come in the form of discrete vectors rather than smooth functions. We thus proceed to discretize Equation 9 as

$$\begin{aligned} \mathbf{Y} &= 2\mathcal{S}\mathbf{\Delta\Sigma} + \mathcal{S}\mathcal{D}\mathbf{\Delta\Sigma} \\ &= \mathcal{T}\mathbf{\Delta\Sigma}, \end{aligned} \tag{10}$$

Here, $\mathcal{D}$ is the matrix of finite difference coefficients for discretized differentiation with respect to $\ln R$. To construct $\mathcal{D}$, we use finite difference schemes that vary according to the location of interest. For a data vector $\mathbf{\Delta\Sigma} = \{\Delta\Sigma_i\}$ with $1 \leq i \leq N$, we use forward/backward schemes of width 4 respectively for $i = 1$ and N, and central schemes of width $\min(i, N-i, 4)$ for the rest. $\mathcal{S}$ represents the trapezoidal summation matrix for discretized integration in $\ln R$. In light of the previous discussions, it is clear that $\mathcal{T} = 2\mathcal{S} + \mathcal{S}\mathcal{D}$ has the property of removing small-scale contributions from $\mathbf{\Delta\Sigma}$. Just as importantly, since $\mathbf{Y}$ is a linear transformation of the original data vector, is is straightforward to compute the covariance matrix of the observable $\mathbf{Y}$,

$$\mathcal{C}_{\mathbf{Y}} = \mathcal{T}\mathcal{C}_{\mathbf{\Delta\Sigma}}\mathcal{T}^{\mathsf{T}}, \tag{11}$$

where $\mathcal{C}_{\mathbf{\Delta\Sigma}}$ is the covariance matrix for $\mathbf{\Delta\Sigma}$. We note that $\mathcal{T}$ has a null mode proportional to $1/R^2$, implying that $\mathcal{T}$ projects out any non-local contribution to $\mathbf{\Delta\Sigma}$ from within the minimum projected radius considered by a given analysis. This can also be seen from adding a $1/R^2$ term to the $\Delta\Sigma$ sector in Eq. 9.

These formulae for constructing $\mathbf{Y}$ and $\mathcal{C}_{\mathbf{Y}}$ can be used to transform any cosmology analysis utilizing $\Delta\Sigma$ as its galaxy–galaxy lensing observable into an analysis that utilizes $\mathbf{Y}$ as its observable. In particular, given a prediction vector $\mathbf{\Delta\Sigma}_{\rm pred}$ and observation vector $\mathbf{\Delta\Sigma}_{\rm obs}$ with covariance matrix $\mathcal{C}_{\mathbf{\Delta\Sigma}}$, we can use $\mathcal{T}$ to obtain $\mathbf{Y}_{\rm pred}$, $\mathbf{Y}_{\rm obs}$, and $\mathcal{C}_{\mathbf{Y}}$. These transformed quantities can then be used for subsequent likelihood analyses in lieu of the original quantities of interest. Moreover, since $\gamma_{\rm t}$ is directly proportional to $\Delta\Sigma$ and $\mathcal{T}$ is a linear transformation, a similar procedure can be applied directly to $\gamma_{\rm t}$, i.e.

$$\mathbf{Y}_\gamma = \mathcal{T}\gamma_{\rm t}, \quad \mathcal{C}_{\mathbf{Y}_\gamma} = \mathcal{T}\mathcal{C}_{\gamma_{\rm t}}\mathcal{T}^{\mathsf{T}}. \tag{12}$$

Now, it is clear that if one used the entire observable data vector $\gamma_{\rm t}$ or $\Delta\Sigma$, a linear transformation will not result in improved cosmological constraints. However, the

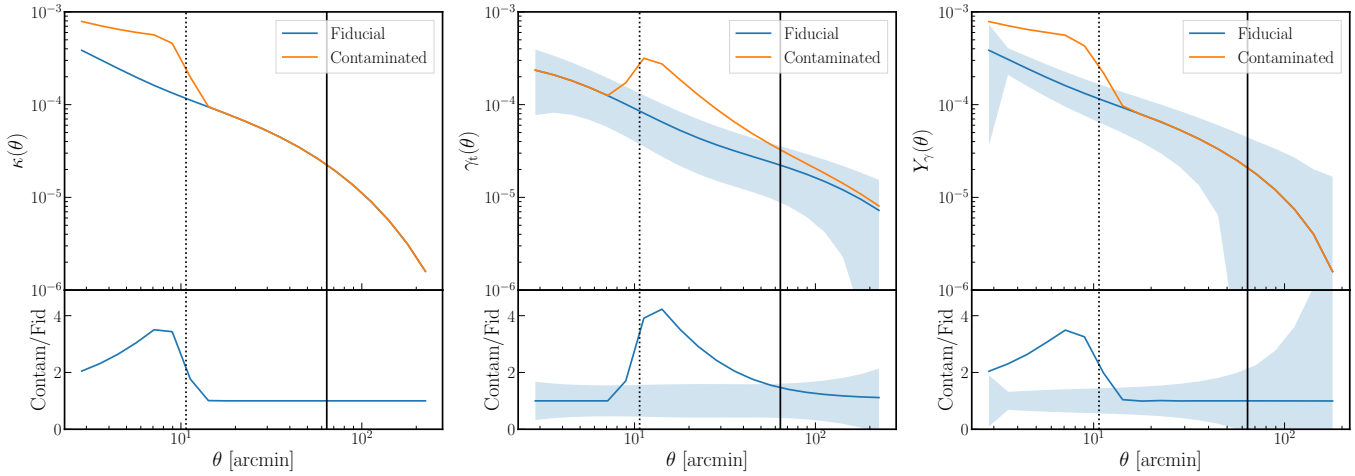

FIG. 1. Comparison of fiducial/contaminated data vectors for quantities κ (left), γ_t (middle), and $\mathbf{Y}_\gamma$ (right). Here, κ is the weak lensing convergence, given by $\kappa(\theta|z_l, z_s) \equiv \Sigma(R = \theta\chi_l)/\Sigma_{\rm crit}(z_l, z_s)$. On each panel, we show the fiducial data vector constructed with linear bias and $\xi_{\rm mm}$ from `halofit` (blue) along with a contaminated data vector with an additional contribution from a disk-like mass profile on small scales (orange). Note that the sharp radial boundary of the disk is smoothed over a range of angular scales due to the breadth of the lens redshift bins for the lenses. The dotted and solid lines respectively represent 2 and 12 h^{-1}Mpc, i.e. $R_{\rm disk}$ and the DES Y1 $R_{\rm min}$, at the representative redshift of the fiducial lens sample. Starting from a localized underlying contamination in κ (left), we observe the non-local propagation of the contamination in γ_t (middle), which is then successfully localized back by the linear transformation $\mathcal{T}$ of Equation 10 (right).

key point here is that all cosmological analyses impose a small scale cut, i.e. we only use a fraction of the observable data vector. By applying the linear transformation derived above, we are able to apply a more aggressive small scale cut, and thereby preserve more of the information relative to a cut in γ_t or $\Delta\Sigma$. In this context, it is also important to emphasize that the transformation matrix $\mathcal{T}$ must be "extended" for combined data vectors consisting of blocks other than galaxy–galaxy lensing. More specifically, we want $\mathcal{T}$ to transform the galaxy–galaxy lensing block while leaving the rest intact in such cases; this can be achieved by extending $\mathcal{T}$ block-diagonally with identity matrices that correspond to the data vector blocks outside of galaxy–galaxy lensing. Defining the transformation matrix across the full combined data vector is important since, in the presence of non-zero covariance between the galaxy–galaxy lensing block and other data blocks in the data vector, Equations 11 and 12 will modify the off-diagonal components of the covariance matrix associated with the galaxy–galaxy lensing block.

III. TESTING THE LOCALITY OF Y

We now test to what extent the new observable Y is local, and whether the improved small scale cuts result in cosmological gains. The methodology for the simulated analyses, closely following [7], is as follows.

1. A simulated data vector is generated from theory with fiducial parameter values. The assumed theoretical model uses the `halofit` [13] nonlinear matter power spectrum and linear galaxy bias.

2. The simulated data vector is "contaminated" with an unmodeled small-scale contribution from a disk-like mass distribution with a constant surface density. The mass of the disk is M and its radius is $R_{\rm disk}$. In terms of $\Delta\Sigma$, the contamination is given by

$$\Delta\Sigma_{\rm disk}(R) = \frac{M}{\pi R^2}\,\Theta(R - R_{\rm disk}). \tag{13}$$

   We propagate this contamination to the γ_t observable, taking into account the lens and source redshift distributions used in [7]. We set $R_{\rm disk} = 2{\rm Mpc}/h$, and adopt masses 4 times larger than those used in [7]. While a disk contamination is not realistic, its sharp boundary best enables us to test whether the observable Y displays non-locality.

3. The simulated contaminated data vector is analyzed without any modeling for the contamination, i.e. assuming the original theoretical model, in order to determine how cosmological inferences are impacted by this contamination.

For all of the considered setups described below, we assume a "2×2pt" cosmological analysis where the observables of interest are $\gamma_t(\theta)$ (galaxy–galaxy lensing) and $w(\theta)$ (galaxy clustering). This combination consists of the minimal set of observables including galaxy–galaxy lensing that breaks the parameter degeneracy between galaxy bias and power spectrum amplitude. Note in particular that this analysis does not incorporate information from cosmic shear, as including cosmic shear will reduce the impact of contaminants in the galaxy–galaxy

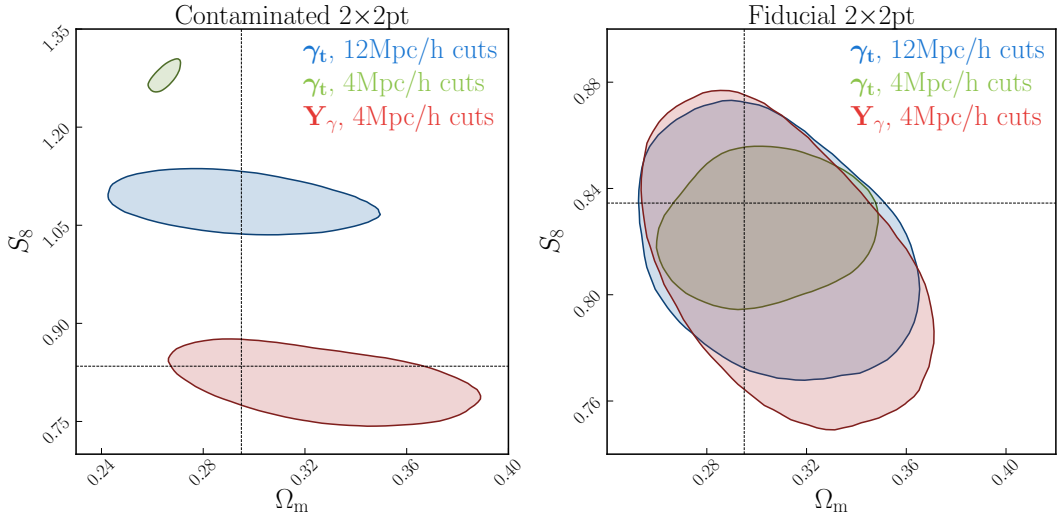

FIG. 2. The 68% confidence regions of the posterior in the Ω_m–S_8 plane, for analyses employing the contaminated (left) and fiducial (right) data vectors, are shown as shaded regions. For each panel, the blue contour corresponds to the baseline analysis described in [1], using γ_t with a 12 h^{-1}Mpc small scale cut. The green and red contours correspond to analyses using γ_t with 4 h^{-1}Mpc cuts and using $\mathbf{Y}$ with 4 h^{-1}Mpc cuts, respectively. Dotted lines denote the fiducial parameter values used to generate the simulated data vectors. Note that the red contours, i.e. the posteriors derived from the $\mathbf{Y}$ observable proposed here, is nearly identical in both panels.

lensing data vector due to the increased "clean" cosmological information drawn from the cosmic shear signal.

We make use of the public DES Y1 analysis pipeline [14] to generate simulated data vectors as well as theory predictions for these observables, and use the public DES Y1 covariances for likelihood calculation. The pipeline is also used to generate Markov Chain Monte Carlo (MCMC) samples for the likelihood analyses, from which we derive parameter constraints over the full DES Y1 parameter space. For more details, we refer the reader to [7]. Here, we will be interested in the bias of the resulting cosmological constraints as the small scale cut used in the analysis of the galaxy–galaxy lensing signal becomes more aggressive.

In Figure 1, we first show the localizing performance of the observable $\mathbf{Y}_\gamma$ by plotting the fiducial and contaminated observables for a single lens-source bin. The left panel shows the local quantity κ, i.e. convergence, underlying the actual observable γ_t. Note that the disk contamination is smoothed beyond $R_{\rm disk}$ due to the width of the lens redshift distribution. The middle panel gives a clear illustration of the non-local behavior of γ_t, where a mass distribution strictly limited to within $R_{\rm disk}$ contaminates the data vector well past the radius $R_{\rm disk}$. The right panel demonstrates the localizing power of $\mathbf{Y}_\gamma$, where we observe that $\mathbf{Y}_\gamma$ can 1) correctly "move back" the contamination to small scales and 2) recover the fiducial input to great accuracy on large scales.

Figure 2 shows the 2D constraints in the $\Omega_m - S_8$ plane from the simulated analyses, where $S_8 = \sigma_8(\Omega_m/0.3)^{0.5}$. The left panel clearly shows both the dangers of the non-locality in galaxy–galaxy lensing, as well as the power of using the localized observable $\mathbf{Y}_\gamma$. Due to the very large contamination employed in this test, even the baseline analysis of the galaxy–galaxy lensing signal γ_t with a conservative small scale cut of 12 h^{-1}Mpc shows highly biased results. The incurred bias is, unsurprisingly, much stronger for the γ_t analysis with 4 h^{-1}Mpc cuts. By contrast, we see that the use of the observable $\mathbf{Y}_\gamma$ results in unbiased cosmological posteriors down to the same small scale cut of 4 h^{-1}Mpc. We stress that our method is agnostic to the type of contamination introduced. It is solely the localizing nature of $\mathbf{Y}_\gamma$ that is driving the debiasing exhibited in Fig. 2.

The right panel shows the bias-variance tradeoff incurred by our approach. In particular, we now analyze an uncontaminated data vector for γ_t with 4 h^{-1}Mpc and 12 h^{-1}Mpc cuts, and compare it to a $\mathbf{Y}_\gamma$ data vector with a 4 h^{-1}Mpc scale cut. Note that the cosmological posteriors for the γ_t data vector with a 12 h^{-1}Mpc cut are tighter than the posteriors for the $\mathbf{Y}_\gamma$ data vector with a 4 h^{-1}Mpc cut. Evidently, for a given scale cut, the $\mathbf{Y}_\gamma$ data vector contains significantly less information than the γ_t data vector. Importantly, however, by construction, the $\mathbf{Y}_\gamma$ data vector should contain all of the information we can adequately model, and no information from scales that we are unable to properly model, a property that the γ_t data vector does not share.

Finally, we test our method for robustness against noise. To do so, we analyze multiple independent noise realizations of the $\mathbf{Y}_\gamma$ data vector. We first generate 100 noisy realizations of the full fiducial data vector (i.e. γ_t and w) from the full fiducial covariance matrix, add the disk contamination to the γ_t section of each realization, and transform γ_t to $\mathbf{Y}_\gamma$. We then perform a grid-based likelihood analysis for each realization, fixing all

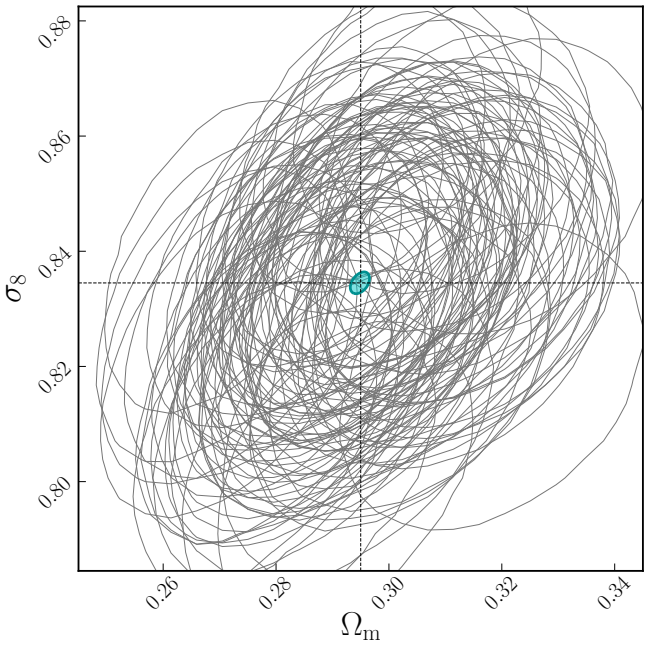

FIG. 3. Constraints on the $\Omega_{\rm m}$–σ_8 plane from simulated "2×2pt" analyses utilizing $\mathbf{Y}_\gamma$, performed on 100 independent noisy realizations of the contaminated data vector. Each gray ellipse represents the resulting posterior for the 2D parameter space from a given noise realization. The filled cyan ellipse represents the combined constraints from all 100 noise realizations, and is consistent with the fiducial parameter values marked by dotted lines.

cosmological and systematics parameters except for $\Omega_{\rm m}$ and σ_8. The analysis relies on the observable $\mathbf{Y}_\gamma$ with a 4 h^{-1}Mpc small scale cut.The results from the noise realization tests are shown in Fig. 3. We find that the parameter constraints from independent noise realizations scatter around the fiducial parameter values, and in addition that the combined constraints from all 100 noise realizations are also consistent with the fiducial values. This shows that the transformations of the data vectors and covariances we introduce in our method are robust against random noise.

IV. SUMMARY AND DISCUSSION

We have introduced a novel observable to mitigate the non-locality in the galaxy–shear correlation function. Our approach is inspired by the local quantity Σ underlying the direct observables $\gamma_{\rm t}$ and $\Delta\Sigma$, and takes the form of a linear transformation on the observable vectors. By utilizing our localized observable $\mathbf{Y}$, we have obtained unbiased cosmological posteriors even under aggressive small-scale cuts in galaxy–galaxy lensing. Our approach is trivial to implement: starting from an existing analysis pipeline, one only needs to add a few matrix multiplications to the observables and the covariance matrices prior to computing the likelihood. Most importantly, our approach ensures that the entirety of the signal used to place cosmological constraints is free of non-local contributions from the small-scale regime, and consequently that the resulting cosmological constraints depend exclusively on accurately modeled physics.

ACKNOWLEDGMENTS

YP was partially supported by the DOE grant DE-SC0015975 and the World Premier International Research Center Initiative (WPI), MEXT, Japan, during the performance of this work. ER was supported by DOE grant DE-SC0015975, and by the Cottrell Scholar program of the Research Corporation for Science Advancement. EK was supported by DOE grant DE-SC0020247.

[1] Dark Energy Survey Collaboration *et al.*, Phys. Rev. D **98**, 043526 (2018), arXiv:1708.01530 [astro-ph.CO].
[2] S. Joudaki, C. Blake, A. Johnson, A. Amon, M. Asgari, A. Choi, T. Erben, K. Glazebrook, J. Harnois-Déraps, C. Heymans, H. Hildebrand t, H. Hoekstra, D. Klaes, K. Kuijken, C. Lidman, A. Mead, L. Miller, D. Parkinson, G. B. Poole, P. Schneider, M. Viola, and C. Wolf, MNRAS **474**, 4894 (2018), arXiv:1707.06627 [astro-ph.CO].
[3] E. van Uitert *et al.*, MNRAS **476**, 4662 (2018), arXiv:1706.05004 [astro-ph.CO].
[4] C. Hikage *et al.*, Publ. Aston. Soc. Jpn. **71**, 43 (2019), arXiv:1809.09148 [astro-ph.CO].
[5] R. Mandelbaum, A. Slosar, T. Baldauf, U. Seljak, C. M. Hirata, R. Nakajima, R. Reyes, and R. E. Smith, MNRAS **432**, 1544 (2013), arXiv:1207.1120 [astro-ph.CO].
[6] V. Desjacques, D. Jeong, and F. Schmidt, Phys. Rept. **733**, 1 (2018), arXiv:1611.09787 [astro-ph.CO].
[7] E. Krause *et al.*, arXiv e-prints , arXiv:1706.09359 (2017), arXiv:1706.09359 [astro-ph.CO].
[8] T. Baldauf, R. E. Smith, U. Seljak, and R. Mand elbaum, Phys. Rev. D **81**, 063531 (2010), arXiv:0911.4973 [astro-ph.CO].
[9] R. Mandelbaum, A. Slosar, T. Baldauf, U. Seljak, C. M. Hirata, R. Nakajima, R. Reyes, and R. E. Smith, MNRAS **432**, 1544 (2013), arXiv:1207.1120 [astro-ph.CO].
[10] N. MacCrann, J. Blazek, B. Jain, and E. Krause, arXiv e-prints , arXiv:1903.07101 (2019), arXiv:1903.07101 [astro-ph.CO].
[11] N. Kaiser, ApJ Letters **439**, L1 (1995), astro-ph/9408092.
[12] D. E. Johnston, E. S. Sheldon, A. Tasitsiomi, J. A. Frieman, R. H. Wechsler, and T. A. McKay, Astrophys. J. **656**, 27 (2007), arXiv:astro-ph/0507467 [astro-ph].
[13] R. Takahashi, M. Sato, T. Nishimichi, A. Taruya, and M. Oguri, Astrophys. J. **761**, 152 (2012), arXiv:1208.2701

[astro-ph.CO].

[14] https://bitbucket.org/joezuntz/cosmosis/wiki/Home.